



**HAL**  
open science

## Measurement report: Ammonia in Paris derived from ground-based open-path and satellite observations

Camille Viatte, Nadir Guendouz, Clarisse Dufaux, Arjan Hensen, Daan Swart, Martin van Damme, Lieven Clarisse, Pierre-François Coheur, Cathy Clerbaux

### ► To cite this version:

Camille Viatte, Nadir Guendouz, Clarisse Dufaux, Arjan Hensen, Daan Swart, et al.. Measurement report: Ammonia in Paris derived from ground-based open-path and satellite observations. Atmospheric Chemistry and Physics Discussions, In press, 10.5194/egusphere-2023-963 . insu-04135233v1

**HAL Id: insu-04135233**

**<https://insu.hal.science/insu-04135233v1>**

Submitted on 20 Jun 2023 (v1), last revised 18 Dec 2023 (v2)

**HAL** is a multi-disciplinary open access archive for the deposit and dissemination of scientific research documents, whether they are published or not. The documents may come from teaching and research institutions in France or abroad, or from public or private research centers.

L'archive ouverte pluridisciplinaire **HAL**, est destinée au dépôt et à la diffusion de documents scientifiques de niveau recherche, publiés ou non, émanant des établissements d'enseignement et de recherche français ou étrangers, des laboratoires publics ou privés.





11 **Abstract**

12 Ammonia (NH<sub>3</sub>) is an important air pollutant which, as precursor of fine particulate matter, raises  
13 public health issues. This study analyzes 2.5-years of NH<sub>3</sub> observations derived from ground-based  
14 (miniDOAS) and satellite (IASI) remote sensing instruments to quantify, for the first time, temporal  
15 variabilities (from interannual to diurnal) of NH<sub>3</sub> concentrations in Paris.

16 The IASI and miniDOAS datasets are found to be in relatively good agreement ( $R > 0.70$ ) when  
17 atmospheric NH<sub>3</sub> concentrations are high and driven by regional agricultural activities. Over the  
18 investigated period (January 2020 – June 2022), NH<sub>3</sub> average concentrations in Paris measured by the  
19 miniDOAS and IASI are 2.23  $\mu\text{g}\cdot\text{m}^{-3}$  and  $7.10 \times 10^{15}$  molecules $\cdot\text{cm}^{-2}$ , respectively, which are lower or  
20 equivalent to those documented in urban areas. The seasonal and monthly variabilities of NH<sub>3</sub>  
21 concentrations in Paris are driven by sporadic agricultural emissions influenced by meteorological  
22 conditions, with NH<sub>3</sub> concentrations in spring up to 2 times higher than in other seasons.

23 The potential source contribution function (PSCF) reveals that the close (100-200km) east and  
24 northeast regions of Paris constitute the most important potential emission source areas of NH<sub>3</sub> in the  
25 megacity.

26 Weekly cycles of NH<sub>3</sub> derived from satellite and ground-based observations show different ammonia  
27 sources in Paris. In spring, agriculture has a major influence on ammonia concentrations and, in the  
28 other seasons, multi-platform observations suggest that ammonia is also controlled by traffic-related  
29 emissions.

30 In Paris, the diurnal cycle of NH<sub>3</sub> concentrations is very similar to the one of NO<sub>2</sub>, with morning  
31 enhancements coincident with intensified road traffic. NH<sub>3</sub> evening enhancements synchronous with  
32 rush hours are also monitored in winter and fall. NH<sub>3</sub> concentrations measured during the weekends  
33 are consistently lower than NH<sub>3</sub> concentrations measured during weekdays in summer and fall. This is  
34 a further evidence of a significant traffic source of NH<sub>3</sub> in Paris.



35 **1. Introduction**

36 Ammonia (NH<sub>3</sub>) is an air pollutant which is involved in important environmental and health issues  
37 [Rockström et al., 2009]. It is a highly reactive gas, with a lifetime of a few hours to a few days  
38 [Evangelou et al., 2021; Dammers et al., 2019], capable of reacting with nitrogen oxides (NO<sub>x</sub>) and  
39 sulfur oxides (SO<sub>x</sub>) to form fine particulate matter composed of ammonium nitrate and ammonium  
40 sulfate [Sutton et al., 2013]. The formation of fine particles plays a major role in the degradation of air  
41 quality, as they are the cause of respiratory and cardiovascular diseases [Pope III et al., 2009].

42 Models have difficulty predicting events of particulate pollution associated with NH<sub>3</sub> since ground-  
43 based atmospheric observations of this gas are still relatively sparse [Nair and Yu, 2020] and difficult  
44 to implement [Twigg et al., 2022; von Bobruzki et al., 2010]. To our knowledge, only six countries in  
45 the world (United States, China, the Netherlands, United Kingdom, Belgium, and Canada) have  
46 dedicated NH<sub>3</sub> observations in their atmospheric monitoring networks. This poses a problem for long-  
47 term monitoring of pollution and the implementation of emission reduction policies.

48 Global population growth causes increased food demand leading to higher ammonia emissions from  
49 intensive agricultural production systems [Fowler et al., 2013]. Global NH<sub>3</sub> emissions have increased  
50 by more than 80% between 1970 and 2017 [McDuffie et al., 2020]. In Europe, a substantial increase in  
51 nitrate and ammonium concentrations in the composition of fine particles has been observed for several  
52 years in the early spring when fertilizer applications intensify [Favez et al., 2021]. In addition, the share  
53 of emissions related to road traffic is also increasing because of popularization of catalytic converters  
54 in car engines [Zhang et al., 2021]. In France, 98% of ammonia comes from agricultural activities, via  
55 decomposition and volatilization of nitrogen fertilizers (34%) and animal waste (64%), the rest are from  
56 industry, road traffic and residential heating [CITEPA, 2022]. In the Ile-de-France region (Paris greater  
57 area), the share of agriculture is lower (75%) due to a higher contribution of traffic and residential  
58 sectors (13% and 12%, respectively [AirParif, 2022]). NH<sub>3</sub> emissions from road traffic are very poorly  
59 quantified and may be a larger than expected source in urban areas [Pu et al., 2023; Chatain et al.,  
60 2022; Cao et al., 2021; Roe et al., 2004; Sutton et al., 2000].

61 Monitoring NH<sub>3</sub> is therefore essential, especially in urban areas such as in Paris, where particulate  
62 pollution episodes are monitored almost every spring [Viatte et al., 2021; Viatte et al., 2020; Petetin  
63 et al., 2016].

64 Global scale measurement of atmospheric ammonia is possible via soundings from several satellite-  
65 borne instruments such as AIRS [Warner et al., 2016], CrIS [Shephard and Cady-Pereira, 2015], and IASI  
66 [Clarisse et al., 2009]. Satellite measurements of atmospheric ammonia allow a description of its spatial  
67 distribution with global coverage. The detection of the multi-year evolution of concentrations is  
68 possible, as well as the detection of emission sources at the kilometer scale [Van Damme et al., 2018],  
69 and even the quantification of their variabilities [Van Damme et al., 2021; Dammers et al., 2019].  
70 Remote sensing data are also used as a mean to estimate ammonia emission inventories [Marais et  
71 al., 2021; Cao et al., 2020; Fortems-Cheiney et al., 2020].

72 Quantifying and analyzing temporal NH<sub>3</sub> variabilities at different scales (diurnal, weekly, seasonal, and  
73 interannual) helps to improve emission inventories and air quality forecasts [Cao et al., 2021]. Diurnal  
74 NH<sub>3</sub> variability, which is rarely measured, is particularly crucial because atmospheric models have  
75 difficulty representing it [Lonsdale et al., 2017]. NH<sub>3</sub> concentrations increase during the day due to the  
76 temperature dependence of emissions, but there may be many other factors at play influencing the



77 diurnal variability of  $\text{NH}_3$  concentrations in the atmosphere, such as transport, boundary layer height,  
78 deposition, fertilizer application time, road traffic emissions, and the interaction of all these factors  
79 [Sudesh and Kulshrestha, 2021; Osada, 2020; Wang et al., 2015]. The diurnal variability of  $\text{NH}_3$ , which  
80 is still largely missing from the ground and satellite observations, provides valuable information  
81 regarding sources, surface exchange, deposition, gas-particle conversion, and transport of  $\text{NH}_3$   
82 [Clarisse et al., 2021].

83 In this work, we present 2.5-years of atmospheric  $\text{NH}_3$  concentrations measured in Paris using the  
84 synergy of ground-based and IASI satellite observations to quantify  $\text{NH}_3$  variabilities at different time  
85 scales.

## 86 **2. Methodology**

### 87 **2.1. mini-DOAS**

88 The miniDOAS (Differential Optical Absorption Spectroscopy) is a state-of-art instrument suitable for  $\text{NH}_3$   
89 monitoring [Berkhout et al., 2017] since it performs accurate high temporal resolution measurements  
90 (every hour, day and night) [Volten et al., 2012]. It has been designed and developed by the National  
91 Institute for Public Health and the Environment (RIVM, Netherlands) to be part of the Dutch National  
92 Air Quality Monitoring Network [Berkhout et al., 2017]. The miniDOAS is an active remote sensing  
93 instrument based on open-path differential absorption spectrometry. It uses a xenon lamp which emits  
94 a UV light, ammonia having a strong absorption band in the UV between 200 and 230 nm. The UV light  
95 beam travels along an optical path of 20 m, at the end of which there is a reflector which reflects the  
96 UV light and sends it back to the spectrometer/receiver. The Beer-Lambert law is used to quantify the  
97 extinction at the absorption wavelengths of ammonia to retrieve atmospheric ammonia  
98 concentrations [Volten et al., 2012]. The miniDOAS can measure a wide range of ammonia  
99 concentrations (from 0.5 to 200  $\mu\text{g.m}^{-3}$ ) day and night with no sampling artifacts, since it is not using  
100 any filter or inlet unlike other instruments [Caville et al., 2023; von Bobruzki et al., 2010]. Estimated  
101 errors are  $4.10^{-3} \mu\text{g.m}^{-3}$  on hourly measurements [Volten et al., 2012]. Using ammonia measurements  
102 performed from the miniDOAS at the QUALAIR super-site (40 meters above ground level,  
103 <https://qualair.fr/index.php/en/english/>) in the Paris city-center, the  $\text{NH}_3$  contribution in particulate  
104 pollution events that occurred during the 2020 COVID lockdown has been demonstrated [Viatte et al.,  
105 2021].

### 106 **2.2. IASI**

107 The Infrared Atmospheric Sounding Interferometer (IASI, [Clerbaux et al., 2009]) was launched first in  
108 2006 as part of the Metop satellite series to monitor atmospheric composition twice a day (at 9:30 and  
109 21:30) globally. IASI measures atmospheric spectra in the thermal infrared region with an elliptical  
110 pixel footprint of  $12 \times 12$  km at nadir and  $20 \times 39$  km at the far end of the swath. In this study, we use  
111  $\text{NH}_3$  columns derived from IASI morning (9:30) overpasses onboard Metop B and C from January 2020  
112 to June 2022. When comparing IASI and miniDOAS  $\text{NH}_3$  concentrations in Paris, we have selected  
113 coincident observations made within the same hour. In this work, we use version 3 of the ANNI- $\text{NH}_3$   
114 reanalyzed dataset [Van Damme et al., 2021; Guo et al., 2021; Viatte et al., 2022].

### 115 **2.3. Meteorological data from ERA-5**

116 Meteorological parameters originate from the ERA-5 database of the European Centre for Medium-  
117 Range Weather Forecasts (ECMWF, [Hersbach et al., 2020]). It is constituted from observations



118 recalibrated on global data assimilation models at a 30km spatial resolution. In this work, we used the  
119 hourly data of the temperature at 2 m, the precipitation, the u and v components of the wind at 100  
120 m and the height of the boundary layer, taken from the grid cells in which Paris is located.

#### 121 **2.4. Back-trajectories and Potential Source Contribution Factor (PSCF) analysis**

122 To study the transport affecting concentration of ammonia in Paris, we use the Hybrid Single-Particle  
123 Lagrangian Integrated Trajectory model (HYSPLIT, [Stein et al., 2015]) to calculate backward  
124 trajectories of air masses ending at altitudes of 100 m (above sea level which corresponds to the  
125 altitude of the miniDOAS location) between January 2020 and June 2022.

126 Meteorological data used in the runs are from the National Centers for Environmental Prediction  
127 (NCEP) / National Center for Atmospheric Research (NCAR) reanalysis at 2.5-degree global latitude-  
128 longitude projection. We ensure by visual inspections that the back trajectories using a 2.5° resolution  
129 meteorological dataset are similar to using a finer meteorological dataset at 0.25° resolution (GFS).

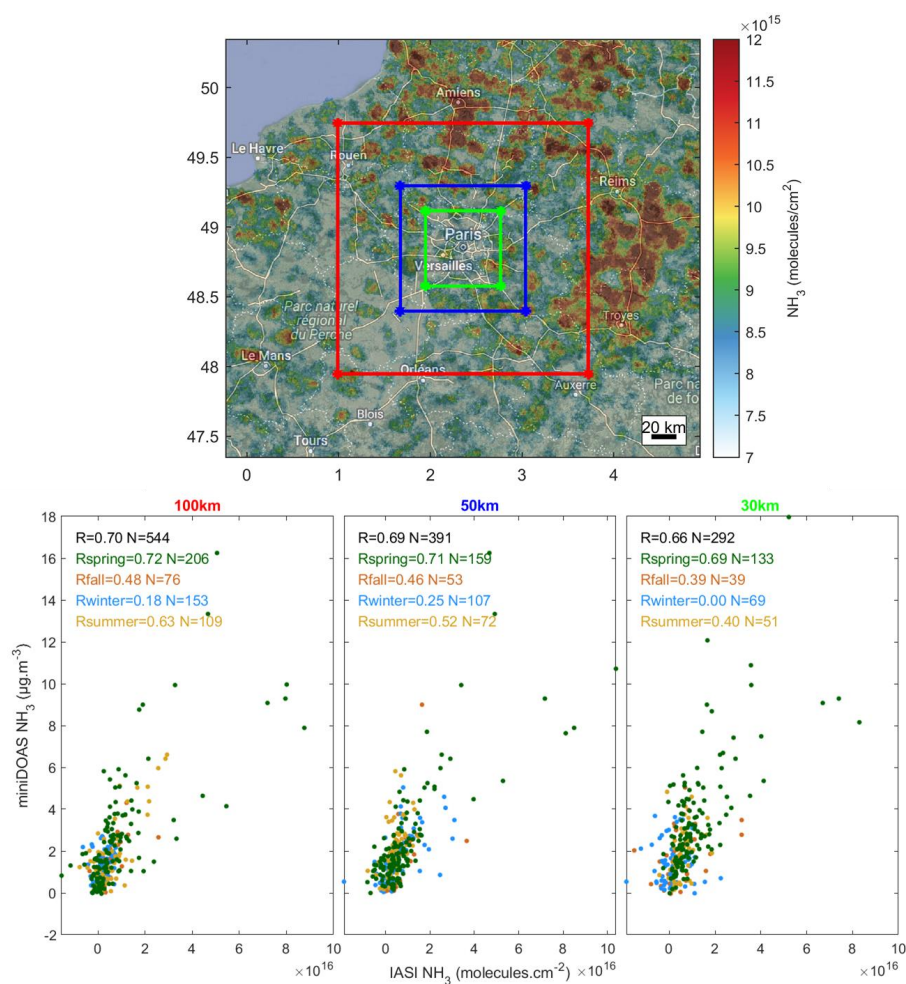
130 Due to the short and highly variable lifetime of NH<sub>3</sub>, ranging between 2-4 hours [Dammers et al., 2019]  
131 and 12-hours [Evangelidou et al., 2021], we simulated an average 6-h backward trajectories with an  
132 interval of one hour. Combining the hourly NH<sub>3</sub> observations from the miniDOAS, the potential  
133 emission sources of NH<sub>3</sub> were analyzed. The Potential Source Contribution Factor (PSCF) method  
134 [Malm et al., 1986] is used to identify source regions affecting air quality in term of NH<sub>3</sub> concentration  
135 in Paris between January 2020 and June 2022. This method is now commonly used in atmospheric  
136 science [Wang et al., 2023; Qadri et al., 2022; Martino et al., 2022; Biuki et al., 2022; Ren et al., 2021;  
137 Zachary et al., 2018; Jeong et al., 2011] and combines the concentration dataset with air parcel back-  
138 trajectory to identify preferred pathways producing high observed NH<sub>3</sub> concentrations in Paris. The  
139 larger PSCF (range: 0–1), the greater contribution of the pollution region to the atmospheric pollutants  
140 at the receptor site.



141 **3. Results**

142 **3.1. Comparison of NH<sub>3</sub> concentrations between IASI and mini-DOAS**

143 The 2.5-years mean NH<sub>3</sub> total column distribution around Paris derived from IASI from January 1<sup>st</sup> 2020  
 144 to May 31<sup>st</sup> 2022 is shown in Figure 1 (top panel). To obtain averages at a high resolution needed for  
 145 city-scale studies, we used the oversampling method that takes into account the real elliptical sizes of  
 146 each IASI pixel [Van Damme et al., 2018]. Hot spots of ammonia are found around Paris in agricultural  
 147 areas, especially in the Champagne-Ardennes region between Troyes and Reims cities [Viatte et al.,  
 148 2020].



149

150 *Figure 1: Top panel: 2.5-years average of IASI NH<sub>3</sub> column distributions (from January 1<sup>st</sup> 2020 to May*  
 151 *31<sup>st</sup> 2022). Bottom panel: miniDOAS ground-based NH<sub>3</sub> concentrations (µg.m<sup>-3</sup>) versus IASI-retrieved*  
 152 *NH<sub>3</sub> column concentrations (molecules.cm<sup>-2</sup>) per season for different spatial criteria from Paris city*  
 153 *center where the miniDOAS is located (100km in red box, 50km in blue box, and 30km green box).*



154 NH<sub>3</sub> has a short atmospheric lifetime which is why we only compare miniDOAS data recorded within  
155 the same hour as the IASI morning overpass time. The IASI-retrieved column (in molecules.cm<sup>-2</sup>) and  
156 the miniDOAS ground-based concentrations (µg.m<sup>-3</sup>) are qualitatively compared to assess the spatial  
157 criteria (100km in red box, 50km in blue box, and 30km green box) and the season for which both  
158 datasets are in best agreement. In this study we are not converting IASI columns to surface  
159 observations since it introduces additional errors and does not change the correlation as explained in  
160 [Van Damme et al., 2015].

161 Overall, the miniDOAS and IASI NH<sub>3</sub> concentrations are in moderate agreement with Pearson  
162 correlation [Akoglu et al., 2018] of 0.70, 0.69, and 0.66 when considering IASI pixels within a 100km,  
163 50km, and 30km box around Paris, respectively. The number of pairs is, however, reduced by a factor  
164 of two when considering IASI pixels in a 100km versus a 30km box around Paris. All correlations are  
165 significant (p-value < 0.05) except in winter for the 100km and 30km boxes, and in fall for the 30km  
166 box. The best agreement between the miniDOAS and IASI is in spring, with Pearson correlations ranging  
167 from 0.72 to 0.69 (green points in scatter plots of Figure 1). This period corresponds to high  
168 atmospheric NH<sub>3</sub> concentrations when spreading practices occur in the surrounding agricultural  
169 regions of Paris [Viatte et al., 2022]. In fall and summer, the Pearson correlation coefficients range  
170 from 0.63 to 0.40 between IASI and the miniDOAS for all boxes sizes. In winter, the agreements are  
171 poor between the miniDOAS and IASI because NH<sub>3</sub> concentrations are weak and IASI is less sensitive  
172 to lower atmospheric layers when thermal contrast is low [Van Damme et al., 2014]. In addition, we  
173 demonstrate that correlations between satellite and ground-based NH<sub>3</sub> observations are independent  
174 of atmospheric temperature and planetary boundary layer height (PBLH, Figure S1).

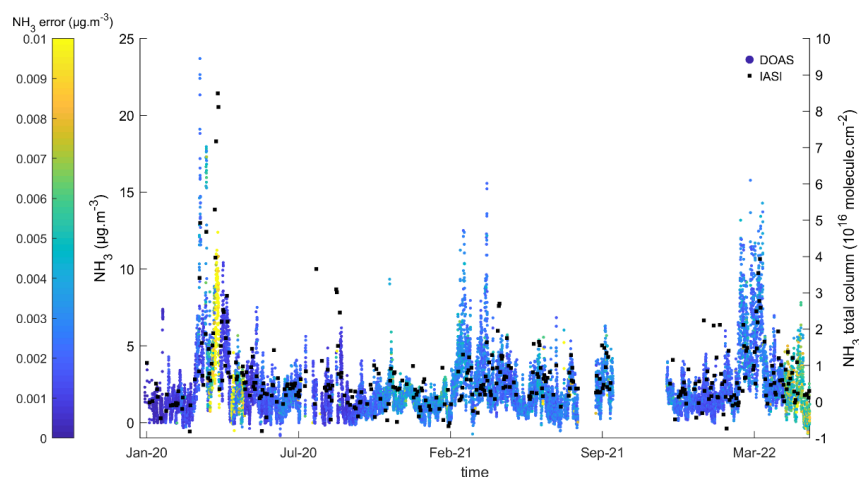
175 A trade-off between good correlations and keeping a sufficient number of collocations is found when  
176 comparing NH<sub>3</sub> concentrations from ground-based measurements located in the Paris city-center with  
177 the IASI dataset in a 50 km box. We chose for the rest of the analysis IASI dataset within the 50 km box  
178 to analyze spatiotemporal variabilities of NH<sub>3</sub> in Paris.

## 179 **3.2. Impact of agriculture on NH<sub>3</sub> concentrations in Paris**

### 180 **3.2.1 2.5-years of NH<sub>3</sub> measurements in Paris**

181 Here, we investigate temporal variabilities of NH<sub>3</sub> using 2.5-years of hourly measurements from  
182 January 1<sup>st</sup> 2020 to May 31<sup>st</sup> 2022 (Figure 2). The miniDOAS was working almost full time during this  
183 period with 16 888 hourly measurements, out of the 21 145 possible. The missing data is due either to  
184 some technical issues during warm conditions (malfunctioning aircondition in August 2021) or due to  
185 its removal from the QUALAIR facility for field measurement campaigns (from September 15<sup>th</sup> 2021 to  
186 November 24<sup>th</sup> 2021). Over the 16 888 hourly NH<sub>3</sub> measurements, average errors are 2.8 10<sup>-3</sup> µg.m<sup>-3</sup>  
187 with maximum values occurring when signal is low due to a transient poor alignment (such as in April  
188 2020, yellow dots in Figure 2).





189

190 *Figure 2: Timeseries of hourly NH<sub>3</sub> concentrations (in µg.m<sup>-3</sup>) color coded by the errors on*  
 191 *measurements derived from the miniDOAS located in Paris, and IASI NH<sub>3</sub> total columns (in black,*  
 192 *molecule.cm<sup>-2</sup>) observed in a 50km box centered in Paris from January 1<sup>st</sup> 2020 to May 31<sup>st</sup> 2022.*

193 The measurements made by the miniDOAS over the period January 2020 - June 2022 (N=16 888) show  
 194 an average ammonia concentration of 2.23 µg.m<sup>-3</sup> in Paris over this period, with a standard deviation  
 195 of 2.02 µg.m<sup>-3</sup>, indicating a high NH<sub>3</sub> variability. In comparison, the average concentration measured  
 196 by the miniDOAS in an agricultural site at Grignon [Loubet et al., 2022] in September–October 2021  
 197 (France) is 6.52 ± 8.44 µg.m<sup>-3</sup> [Claville et al., 2023], almost three times higher than in Paris. The  
 198 relatively low concentrations observed in Paris are explained by the distance to the major emission  
 199 sources which are related to agricultural activities. Ammonia concentrations measured in Paris are on  
 200 average lower or equivalent to those documented in urban areas such as Beijing (China, 21 ± 14 ppb  
 201 corresponding to 14.7 ± 10 µg.m<sup>-3</sup> from January 2018 to January 2019, [Lan et al., 2021]), Shanghai  
 202 (China, 6.2 ± 4.6 ppb which corresponds to 4.3 ± 3.2 µg.m<sup>-3</sup> from July 2013 to September 2014, [Wang  
 203 et al., 2015]), Rome (Italy, 1.2–21.6 µg.m<sup>-3</sup> between May 2001 and March 2002, [Perrino et al., 2002]),  
 204 Milan (Italy, 4.4–13.4 µg.m<sup>-3</sup> between 2007 and 2019, [Lonati et al., 2020]), Louisville (Unites-States,  
 205 2.2–5.2 µg.m<sup>-3</sup> from June to August 2011, [Li et al., 2017]) and Toronto (Canada, 2.5 ppb which  
 206 corresponds to 1.75 µg.m<sup>-3</sup> from 2003 to 2011, [Hu et al. 2014]).

207 The miniDOAS and IASI coincident measurements show relatively low interannual variability (Table 1).  
 208 NH<sub>3</sub> annual concentrations measured by the miniDOAS are 2.06 ± 2.09 µg.m<sup>-3</sup> and 2.04 ± 1.56 µg.m<sup>-3</sup>  
 209 for 2020 and 2021, respectively. The higher mean and standard deviation in 2022 (2.91 ± 2.40 µg.m<sup>-3</sup>  
 210 for the miniDOAS) compared to the other years can be due the fact that measurements are performed  
 211 from January to June only. IASI NH<sub>3</sub> total columns around Paris exhibit a higher NH<sub>3</sub> annual  
 212 concentration and standard deviation in 2020 compared to the other years because of high pollution  
 213 events occurring in spring during the 2020-COVID lockdown [Viatte et al., 2021].



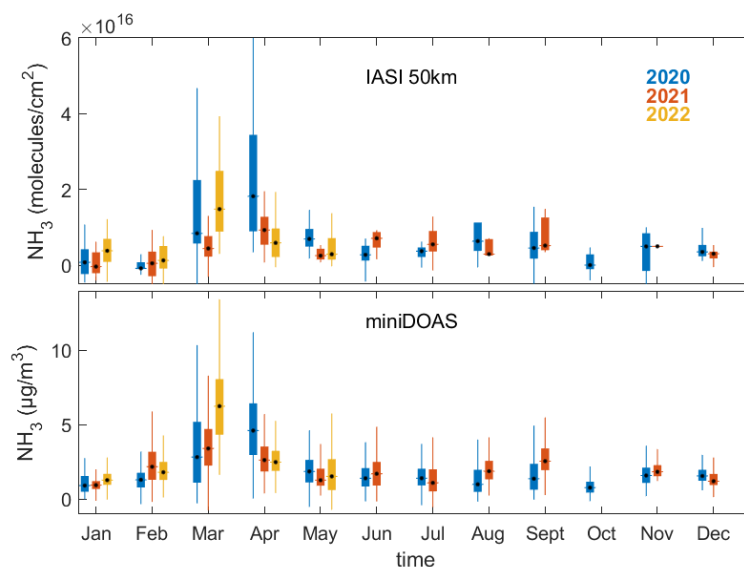
214 *Table 1: Average NH<sub>3</sub> concentration, standard deviation, and number of observations for 2020, 2021*  
 215 *and part of 2022 derived from coincident measurements of the miniDOAS and IASI (50 km box around*  
 216 *Paris).*

years	2020		2021		2022	
	miniDOAS	IASI (50km)	miniDOAS	IASI (50km)	miniDOAS	IASI (50km)
NH <sub>3</sub> concentration (µg.m <sup>-3</sup> or molecules.cm <sup>-2</sup> )	2.06	8.60 10 <sup>15</sup>	2.04	5.48 10 <sup>15</sup>	2.91	6.76 10 <sup>15</sup>
Standard deviation (µg.m <sup>-3</sup> or molecules.cm <sup>-2</sup> )	2.09	1.58 10 <sup>16</sup>	1.56	5.69 10 <sup>15</sup>	2.40	9.35 10 <sup>15</sup>
Number of observations	7164	166	6182	134	3542	91

217

### 218 3.2.2 Seasonal and monthly NH<sub>3</sub> variabilities in Paris

219 Unlike the weak interannual variability of NH<sub>3</sub> concentrations in Paris, both ground-based (miniDOAS)  
 220 and satellite (IASI) measurements reveal high seasonal variabilities of NH<sub>3</sub> concentrations (Figure 3). In  
 221 spring, NH<sub>3</sub> concentration measured in Paris by the miniDOAS and IASI are on average  
 222  $3.34 \pm 2.67 \mu\text{g.m}^{-3}$  and  $1.21 \times 10^{16} \pm 1.57 \times 10^{16}$  molecules.cm<sup>-2</sup>, respectively. These springtime NH<sub>3</sub>  
 223 concentrations are enhanced by a factor of two compared to the other seasons, which is consistent  
 224 with the fertilizer application periods over the nearby agricultural fields. Both datasets show that NH<sub>3</sub>  
 225 concentrations in March and April are 2 to 3 times higher than the other months. Precipitation for  
 226 these months is also lower than in February on average (see supplementary Figure S2).



227

228 *Figure 3: Monthly NH<sub>3</sub> concentrations color coded by the year of measurements (2020 in blue, 2021 in*  
 229 *orange, and 2022 in yellow) derived from IASI (top panel, in molecules.cm<sup>-2</sup>) in a 50km box around Paris*  
 230 *and the ground-based miniDOAS instrument (bottom panel, in µg.m<sup>-3</sup>) located in Paris city-center. One*  
 231 *note that IASI observations are only considered when a miniDOAS observation is available within the*  
 232 *same hour than IASI overpass.*



233 When considering each year of measurement separately, we notice that the timing of the maximum  
234  $\text{NH}_3$  concentrations is variable. In 2020, the maximum is reached in April with averaged  $\text{NH}_3$   
235 concentrations of  $4.76 \pm 2.48 \mu\text{g.m}^{-3}$  (miniDOAS) and  $2.90 \times 10^{16} \pm 2.85 \times 10^{16}$  molecules. $\text{cm}^{-2}$  (IASI),  
236 whereas in 2022 the maximum appears in March with a monthly  $\text{NH}_3$  concentration of  $6.42 \pm 2.46$   
237  $\mu\text{g.m}^{-3}$  and  $1.72 \times 10^{16} \pm 1.04 \times 10^{16}$  molecules. $\text{cm}^{-2}$  derived from the miniDOAS and IASI, respectively.

238 Meteorological conditions influence the timing of the agricultural practices (farmers do not spread  
239 their fertilizer when it rains),  $\text{NH}_3$  volatilization from the soil to the atmosphere (higher temperature  
240 favors  $\text{NH}_3$  volatilization [Sutton et al., 2013]), and the transport of  $\text{NH}_3$  over Paris.

241 In April 2020,  $\text{NH}_3$  concentrations observed by IASI and the miniDOAS are high compared to April 2022.  
242 In April 2020, precipitation is low (0.3 mm compared to 0.75mm in April 2022) and the monthly  
243 averaged atmospheric temperature is on 3 to 5°C higher than in 2021 and 2022 (Figure S2). This could  
244 explain why  $\text{NH}_3$  concentrations are higher in April 2020 than in 2022. Similarly, the lower ammonia  
245 concentration recorded in March 2021 compared to March 2022 is likely explained by higher  
246 precipitation (0.09 mm) and a lower temperature (of 2°C on monthly average) than in March 2022.

247 In 2021, a second  $\text{NH}_3$  enhancement is measured in September by the miniDOAS ( $2.73 \pm 1.14 \mu\text{g.m}^{-3}$ )  
248 and IASI ( $7.93 \times 10^{15} \pm 4.64 \times 10^{15}$  molecules. $\text{cm}^{-2}$ ). The pronounced seasonal variability can be explained  
249 in the first order by the practices of the farmers. In most European countries, strict regulations are  
250 applied in term of the timing of fertilizer application [Ge et al., 2020]. In France, it is forbidden to spread  
251 nitrogen fertilizers in winter months (between November 30th and February 15<sup>th</sup>, [Ludemann et al.,  
252 2022]) depending on fertilizer and land/crop types.

253 Overall, the seasonal and monthly variabilities of  $\text{NH}_3$  concentrations in Paris are dominated by  
254 agricultural activities and meteorological conditions.

### 255 **3.2.3 Potential Source Contribution Function (PSCF) analysis for $\text{NH}_3$ concentrations**

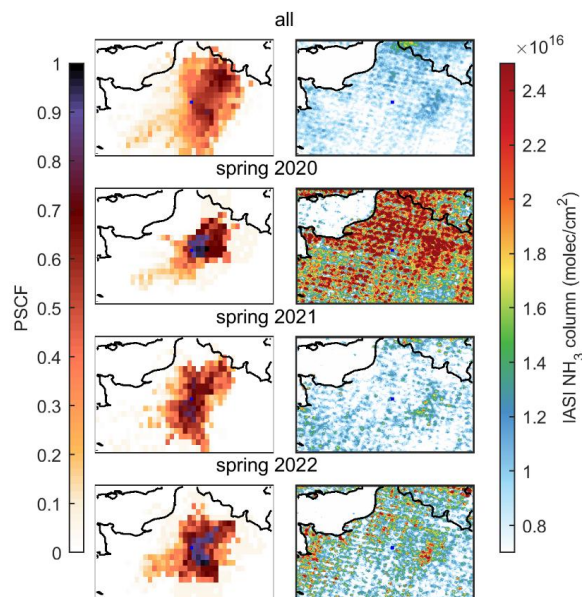
256 To determine the origin of the  $\text{NH}_3$  measured in Paris, the Potential Source Contribution Function  
257 (PSCF) is used. The PSCF analysis, as well as the IASI  $\text{NH}_3$  maps, are shown for the investigated period  
258 (January 2020 – June 2022, Figure 4 upper panels), and for springs 2020, 2021, and 2022 (Figure 4,  
259 three lower panels).

260 Over the whole timeseries, the northeast (100 km from Paris in the Aisne department of France) and  
261 east (70km from Paris in the “Seine et Marne” department) locations are found to affect the  $\text{NH}_3$   
262 concentrations observed in the city between January 2020 and June 2022. These areas are indeed  
263 source regions of  $\text{NH}_3$  according to coincident IASI observations (Figure 4, upper panels). According to  
264 wind fields parameters derived from ERA-5 over Paris (not shown here), the winds from the south are  
265 more intense (up to 18  $\text{m.s}^{-1}$ ) and are related to lower ammonia concentrations (between 0 and 4  $\mu\text{g.m}^{-3}$ ).  
266 The northern winds are on average weaker (maximum around 12  $\text{m.s}^{-1}$ ) and are associated with  
267 higher ammonia concentrations. In particular, for the northeast section the measured  $\text{NH}_3$   
268 concentration is found to exceed 8  $\mu\text{g.m}^{-3}$ .

269 According to the PSCF analysis, the main sources of  $\text{NH}_3$  from agricultural activities are found in the  
270 close areas of Paris (within 100 and 200 km from Paris city-center) mainly from the east and northeast  
271 directions. In France, the averaged utilized agricultural area per department in 2020 is 64.5 ha (Agreste  
272 – Recensements agricoles, <https://stats.agriculture.gouv.fr/cartostat/#c=home>). The highlighted



273 departments by the PSCF analysis are ranked to have the most cultivated areas in France with 141.5  
274 ha for Seine et Marne, 124.4 ha for Oise, and 110.4 ha for Aisne departments for instance.  
275



276 *Figure 4: Potential Source Contribution Function (PSCF, left) and IASI NH<sub>3</sub> total columns (right, in*  
277 *molecules.cm<sup>-2</sup>) The top row is the January 2020 to June 2022 average, and the 3 lower panels are for*  
278 *springs 2020, 2021, and 2022. The blue dot indicates the location of Paris.*  
279

280 In spring, when NH<sub>3</sub> concentrations are significantly higher in Paris (Figure 3) and in the surroundings  
281 (Figure 4 three lower right panels), the PSCF analysis show that the northeast and southeast regions  
282 are the major sources of the observed NH<sub>3</sub> concentrations in Paris. In spring 2020, NH<sub>3</sub> columns are  
283 higher than in spring 2021 and 2022, according to IASI observations. The main sources of NH<sub>3</sub> in spring  
284 2020 are pronounced in the nearby east-northeast areas (at 50 km from Paris in the surrounding  
285 departments of Seine et Marne, Oise, and Val d'Oise). In spring 2021, IASI observations reveal lower  
286 NH<sub>3</sub> columns than in 2020 and 2022 and the sources of NH<sub>3</sub> concentrations in Paris are in the  
287 surrounding regions of Paris (100 km in all directions). In spring 2022, the northeast pathway is  
288 highlighted similarly to spring 2020 but with a contribution of the southeast region as well.



289 **3.3 Effect of road traffic on NH<sub>3</sub> variability in Paris**

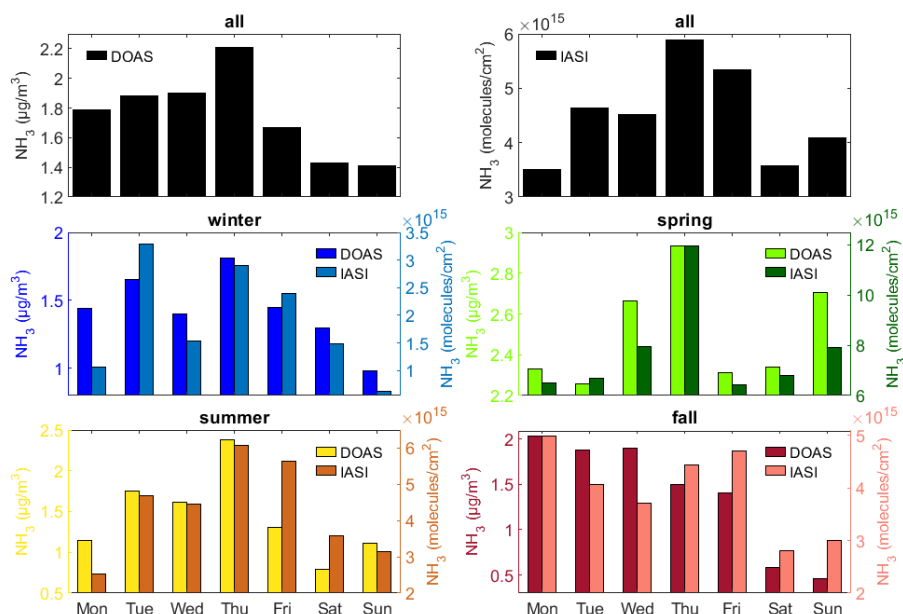
290 **3.3.1 Weekly cycle of NH<sub>3</sub> concentrations**

291 The weekly cycles of ammonia concentrations measured in Paris by the miniDOAS and IASI over the  
292 studied timeseries are presented in Figure 5 (black bars, top panels). Both datasets show an increase  
293 of ammonia concentrations during the week, reaching a maximum on Thursday (2.21 µg.m<sup>3</sup> for the  
294 miniDOAS and 5.90x10<sup>15</sup> molecules.cm<sup>-2</sup> for IASI).

295 The weekly cycle of IASI measurements in Paris is almost analogous to the one observed over European  
296 agricultural areas with low concentrations observed on Mondays and an accumulation of ammonia  
297 during the week [Van Damme et al., 2022]. In addition, the IASI NH<sub>3</sub> weekly cycle averaged over 2.5-  
298 years of measurements in Paris is very similar to the NH<sub>3</sub> weekly cycle measured in spring (Figure 5)  
299 when agricultural activities intensify. Monitoring similar NH<sub>3</sub> weekly variability in the urban area of  
300 Paris demonstrates that agricultural activities in the surrounding areas control the variability of  
301 ammonia in Paris on average over the whole season.

302 The NH<sub>3</sub> weekly cycle observed over 2.5-years of measurements from the ground-based miniDOAS and  
303 the IASI satellite observations show, however, relatively low NH<sub>3</sub> concentrations on Saturday and  
304 Sunday. The cycle is less pronounced for IASI measurements. Ammonia concentrations observed over  
305 the weekend by the miniDOAS and IASI are lower by 25% and 20% compared to NH<sub>3</sub> concentrations  
306 averaged over the weekdays in Paris.

307 When considering intraweek variabilities by seasons (Figure 5, four lower panels), one can observe  
308 that both IASI and the miniDOAS dataset reveal similar NH<sub>3</sub> weekly cycles. The NH<sub>3</sub> miniDOAS  
309 measurements and coincident IASI total columns measured in a 50km box around Paris exhibit lower  
310 concentrations over the weekends compared to weekdays for all seasons, except in spring for which  
311 higher NH<sub>3</sub> concentrations are found on Wednesday and Sunday. In spring, the miniDOAS and IASI  
312 measure a difference of NH<sub>3</sub> concentrations averaged over the weekends compared to weekdays of  
313 +1% and -7%, respectively. In fall, summer, and winter, the miniDOAS (IASI) instrument measure a  
314 decrease of NH<sub>3</sub> concentrations between weekends and weekdays of 70% (34%), 42% (28%), and 27%  
315 (53%) respectively.



316

317 *Figure 5: Day of the week NH<sub>3</sub> concentrations derived from the miniDOAS (µg.m<sup>-3</sup>) and IASI*  
 318 *(molecules.cm<sup>-2</sup>) in Paris for the investigated period (January 2020 to May 2022, top panels), and for*  
 319 *different seasons (winter in blue, spring in green, summer in brown and yellow, and fall in red and pink*  
 320 *bars).*

321 Comparing these weekly variabilities with those of the weekly flow of cars in Paris (Figure S3), the same  
 322 pattern is clearly highlighted with a stable number of cars per hour from Monday to Friday (around  
 323 640) and a decrease of 14% over the weekends.

324 We can make the hypothesis that during all seasons except spring, the influence of the agricultural  
 325 practices on the variability of ammonia in Paris is less pronounced, revealing NH<sub>3</sub> contribution from  
 326 the traffic source. Since the road traffic intensity is constant throughout the year in Paris, the  
 327 proportion of ammonia emitted from road traffic is proportionally higher outside the fertilization  
 328 period.

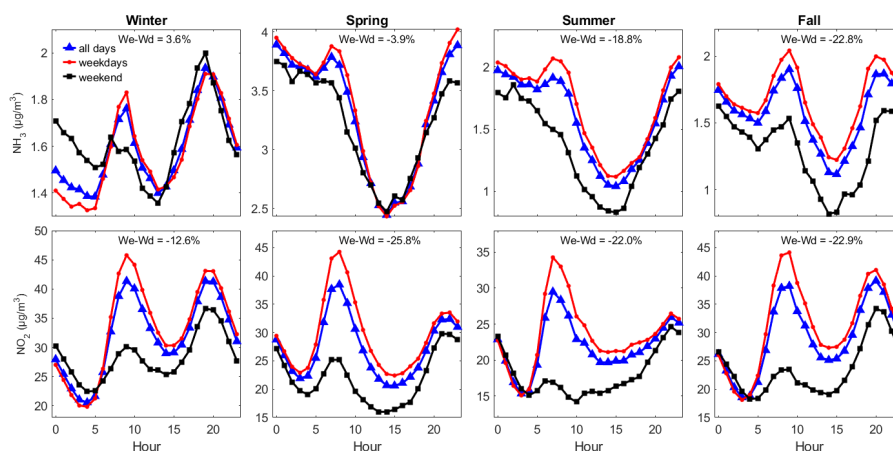
### 329 3.3.2 Diurnal cycle of NH<sub>3</sub> concentration in Paris

330 With the high temporal resolution of the mini-DOAS acquisitions, the diurnal variability of NH<sub>3</sub>  
 331 concentration is assessed in Paris using, for the first time, a quasi-continuous (temporal coverage of  
 332 80%) and a relatively long timeseries of 2.5-years of NH<sub>3</sub> observations.

333 Hourly NH<sub>3</sub> concentrations measured by the miniDOAS from January 2020 to May 2022 are shown in  
 334 Figure S4. It shows a marked diurnal variability of NH<sub>3</sub>, with a decrease of about 30% in the middle of  
 335 the day (around 14:00 LT) compared to the night, then an increase in the afternoon to reach again a  
 336 maximum during the night.



337 Note that this diurnal variability of  $\text{NH}_3$  measured by the miniDOAS is different than the one reported  
 338 during springtime pollution episodes from a ground-based Fourier Transform InfraRed spectrometer  
 339 located in the suburbs of Paris [Kutzner et al., 2021]. While measured integrated  $\text{NH}_3$  total columns  
 340 show an intraday increase until late afternoon, the miniDOAS measures  $\text{NH}_3$  concentrations varying in  
 341 opposition to the boundary layer height (Figure S4). This reflects the dynamical effect of the boundary  
 342 layer height, which is controlled by atmospheric temperature, on the dilution of pollutants  
 343 concentrations measured close to the surface. Such effect is also seen with surface measurements of  
 344  $\text{NO}_2$  concentrations in Paris (Figure S4).



345

346 *Figure 6: Diurnal variability of  $\text{NH}_3$  (upper panels) and  $\text{NO}_2$  (lower panels) concentrations measured by*  
 347 *the miniDOAS and Airparif in ( $\mu\text{g}\cdot\text{m}^{-3}$ ) averaged by seasons using 2.5-years of measurements in Paris.*  
 348 *Hours are indicated in local time. The diurnal variability of  $\text{NH}_3$  and  $\text{NO}_2$  are shown in blue lines when*  
 349 *considering all days, in red lines for weekdays, and in black lines for weekends.*

350 The diurnal variability of  $\text{NH}_3$  concentrations presents an increase in the morning visible for all seasons  
 351 (Figure 6). Between 5:00 and 8:00, road-traffic in Paris increases by a factor 4 (Figure S3) and  $\text{NH}_3$   
 352 concentrations rise by more than 20% in winter and fall, and about 3% in summer and spring.

353 To verify the hypothesis that road traffic is responsible for these morning enhancements,  $\text{NO}_2$  diurnal  
 354 variability is also shown in Figure 6 (lower panels). In Paris,  $\text{NO}_2$  is considered as a proxy for road traffic  
 355 emissions [Pazmino et al., 2022]. For all seasons, morning enhancements of  $\text{NO}_2$  concentrations related  
 356 to intensified road traffic emissions are coincident with morning enhancements of  $\text{NH}_3$  concentrations.  
 357 Similarly, enhancements of  $\text{NO}_2$  and  $\text{NH}_3$  concentrations are observed during the evenings (20:00 to  
 358 22:00 LT) in winter and fall only. In spring, agriculture which is the overall dominant source of ammonia  
 359 in Paris, prevents from monitoring  $\text{NH}_3$  emitted from road traffic. Conversely, in fall and winter, the  
 360 relative share of agriculture is weaker, and the peaks of  $\text{NH}_3$  concentrations during rush hours (morning  
 361 and evening) are clearly observed by the miniDOAS.

362 Diurnal variability of  $\text{NH}_3$  and  $\text{NO}_2$  concentrations averaged during weekdays (red lines) and weekends  
 363 (black lines) are shown in Figure 6.  $\text{NO}_2$  concentrations are systematically lower during weekends by  
 364 12.6%, 25.8%, 22.0%, and 22.9% in winter, spring, summer, and fall respectively, compared to





365 weekdays. Similarly, diurnal cycle of  $\text{NH}_3$  concentrations averaged during weekends are constantly  
366 lower than  $\text{NH}_3$  concentrations averaged during weekdays in summer and fall by 22.0% and 22.9%.

367 This highlights the importance of traffic emissions of  $\text{NH}_3$  in such urban area of Paris, detected by  
368 ground-based measurements when agricultural practices are reduced in the surrounding region.

369 These results are consistent with previous studies showing the importance of  $\text{NH}_3$  emissions from  
370 traffic in urban areas, such as in Rome (Italy, [Perrino et al., 2002]), in Beijing (China, [Ianniello et al.,  
371 2010]), in Shanghai (China, [Wang et al., 2015]), and in Manchester (United Kingdom, [Whitehead et  
372 al., 2004]) for instance. These emissions have gradually become another major contribution of  
373 ammonia pollution in urban areas in the United States and China [Sun et al., 2017]. Ammonia emissions  
374 from road vehicles are shown to be underestimated in the United Kingdom [Farren et al., 2020] and in  
375 densely-populated areas in China [Wen et al., 2022]. In France,  $\text{NH}_3$  levels measured at a traffic site are  
376 significantly higher than those observed in a background site [Chatain et al., 2022]. Our results in Paris  
377 confirm that traffic has a significant contribution to atmospheric nitrogen budgets and stress the need  
378 for further  $\text{NH}_3$  monitoring in urban sites.

#### 379 **4. Conclusion**

380 Atmospheric variabilities of  $\text{NH}_3$  concentrations in Paris are assessed using joined observations of  
381 ground-based (miniDOAS) and satellite (IASI) remote sensing observations from January 2020 to June  
382 2022. We present the first relatively long (2.5-years) and continuous record of hourly  $\text{NH}_3$   
383 concentrations in Paris to determine temporal variabilities of ammonia at different scales (from  
384 interannual to diurnal variability) to unravel emission sources (traffic and agriculture).

385

386 Qualitative comparison of  $\text{NH}_3$  derived from the ground-based miniDOAS located in Paris city-center  
387 and IASI satellite observations reveals an overall moderate agreement with Pearson's correlation  
388 coefficients of 0.66, 0.69 and 0.70 when considering IASI observations in a 100km, 50km, and 30km  
389 box around Paris. The best agreement between both datasets is found during springtime when  $\text{NH}_3$   
390 concentrations are 2 to 3 times higher than during the other seasons due to spreading practices  
391 occurring in the surrounding agricultural regions of Paris. Overall, agricultural activities driven by  
392 favorable meteorological conditions (high temperature and low precipitation) control the seasonal and  
393 monthly variabilities of  $\text{NH}_3$  in Paris. The PSCF analyses indicate that the close east and northeast  
394 agricultural regions (within 100 and 200 km from Paris city-center) affect the most the  $\text{NH}_3$  budget in  
395 Paris.

396

397 Road-traffic emissions are noticeable in the weekly  $\text{NH}_3$  cycles measured by satellite and ground-based  
398 instruments, when agricultural related emissions are weak. Ammonia concentrations observed over  
399 the weekend by the miniDOAS and IASI are lower by 25% and 20% compared to  $\text{NH}_3$  concentrations  
400 averaged over the weekdays. In addition, diurnal cycles of  $\text{NH}_3$  concentrations in Paris are similar to  
401  $\text{NO}_2$  and reveal coincident enhancements during rush hours. Further long-term  $\text{NH}_3$  monitoring in  
402 urban areas is needed to better estimate  $\text{NH}_3$  emissions from the on-road sector and their impact on  
403 secondary particle formation.

404

405 We have shown that the planetary boundary layer height greatly influences diurnal variabilities derived  
406 from surface measurements. Future work will be carried to compare these  $\text{NH}_3$  datasets in Paris to  
407 atmospheric model outputs to evaluate the timing and the absolute value of emission inventories, as





408 well as the partition between NH<sub>3</sub> emission sectors (traffic vs. agriculture). The launch of the  
409 geostationary MTG satellite carrying the hyperspectral sounder IRS, scheduled for 2024, will offer  
410 unprecedented atmospheric observations with a spatial resolution of 4 km × 4 km (at the Equator) and a  
411 high temporal resolution (every 30 minutes over Europe). These new observations will improve our  
412 understanding of the diurnal variability of ammonia, and it will be a great addition to the miniDOAS  
413 and IASI observations.

414

#### 415 **Data availability**

416 The IASI NH<sub>3</sub> dataset used in this study are available via the Zenodo repository  
417 <https://doi.org/10.5281/zenodo.7962362> (Viatte, 2023). The miniDOAS data are available here  
418 [https://iasi-ft.eu/products/nh3\\_minidoas/](https://iasi-ft.eu/products/nh3_minidoas/) (Viatte, 2023). The ERA-5 data are available via the Climate  
419 Data Record (CDR) Copernicus website  
420 <https://cds.climate.copernicus.eu/cdsapp#!/search?text=ERA5%20back%20extension&type=dataset>  
421 (C3S CDS, 2023). The potential source contribution function is available via the Meteothink.org  
422 <http://meteothink.org/docs/trajstat/pscf.html> (Wang et al., 2009). Last access to all URLs: 23 May  
423 2023.

424

#### 425 **Author contributions**

426 CV and NG designed the project. MVD and LC provided the IASI data. AH, AW, DS helped with the  
427 miniDOAS installation and data acquisition. CV and CD analyzed the data. CV and CD wrote the  
428 manuscript draft. All the co-authors reviewed and edited the manuscript. CC wrote proposals to  
429 financially support the miniDOAS.

#### 430 **Competing interests**

431 The authors declare that they have no conflict of interest.

#### 432 **Acknowledgments**

433 IASI is a joint mission of EUMETSAT and the Centre National d'Etudes Spatiales (CNES, France). The IASI  
434 Level 1C data are distributed in near real time by EUMETSAT through the EUMETCast system  
435 distribution. The authors acknowledge the AERIS data infrastructure (<https://www.aeris-data.fr>) for  
436 providing access to the IASI Level 1 radiance and Level 2 NH<sub>3</sub> concentration data used in this study.  
437 CNES and the AC-SAF (CDOP3) project provided financial support for the miniDOAS acquisition. We  
438 thank the NOAA's Air Resources Laboratory (ARL) for providing the HYSPLIT model. Research at ULB  
439 was supported by the Belgian State Federal Office for Scientific, Technical and Cultural Affairs (Prodex  
440 HIRS) and the Air Liquide Foundation (TAPIR project). LC is Research Associate supported by the Belgian  
441 F.R.S.-FNRS. MVD is supported by the FED-tWIN project ARENBERG funded via the Belgian Science  
442 Policy Office (BELSPO).

443



#### 444 **References**

- 445 AERIS: NH<sub>3</sub> total column from IASI (Level 2), <https://iasi.aeris-data.fr/NH3/>, last access: 11 May 2023.
- 446 Airparif, 2022 : <https://www.airparif.asso.fr/surveiller-la-pollution/les-emissions>, last access 24 Feb 2023.
- 447
- 448 Akoglu, H.: User's guide to correlation coefficients, *Turkish J. Emerg. Med.*, 18(3), 91–93, doi:<https://doi.org/10.1016/j.tjem.2018.08.001>, 2018.
- 449
- 450 Berkhout, A. J. C., Swart, D. P. J., Volten, H., Gast, L. F. L., Haaima, M., Verboom, H., Stefess, G.,  
451 Hafkenscheid, T., and Hoogerbrugge, R.: Replacing the AMOR with the miniDOAS in the ammonia  
452 monitoring network in the Netherlands, *Atmos. Meas. Tech.*, 10, 4099–4120,  
453 <https://doi.org/10.5194/amt-10-4099-2017>, 2017.
- 454 Biuki, Z. A., Parvin, P. and Aghaei, M.: Satellite remote sensing of particulate matter in the atmosphere  
455 of megacities: A case study of Tehran, Iran, *Atmos. Pollut. Res.*, 13(10), 101545,  
456 doi:<https://doi.org/10.1016/j.apr.2022.101545>, 2022.
- 457 Cao, H., Henze, D. K., Cady-Pereira, K., McDonald, B. C., Harkins, C., Sun, K., Bowman, K. W., Fu, T.-M.  
458 and Nawaz, M. O.: COVID-19 Lockdowns Afford the First Satellite-Based Confirmation That Vehicles  
459 Are an Under-recognized Source of Urban NH<sub>3</sub> Pollution in Los Angeles, *Environ. Sci. Technol. Lett.*,  
460 doi:10.1021/acs.estlett.1c00730, 2021.
- 461 Cao, H., Henze, D. K., Shephard, M. W., Dammers, E., Cady-Pereira, K., Alvarado, M., Lonsdale, C., Luo,  
462 G., Yu, F., Zhu, L., Danielson, C. G. and Edgerton, E. S.: Inverse modeling of NH<sub>3</sub> sources using CrIS  
463 remote sensing measurements, *Environ. Res. Lett.*, 15(10), 104082, doi:10.1088/1748-9326/abb5cc,  
464 2020.
- 465 Caville et al.: Measurements of ammonia in ambient air and over a controlled artificial source during  
466 the AMICA field campaign at a rural site in the Ile-de-France region, *Sensors*, to be submitted, 2023.
- 467 Chatain, M., Chretien, E., Crunaire, S. and Jantzem, E.: Road Traffic and Its Influence on Urban Ammonia  
468 Concentrations (France), *Atmosphere (Basel)*, 13(7), doi:10.3390/atmos13071032, 2022.
- 469 CITEPA, 2022: [https://www.citepa.org/wp-content/uploads/publications/cee-](https://www.citepa.org/wp-content/uploads/publications/cee-nu/UNECE_France_mars2022.pdf)  
470 [nu/UNECE France mars2022.pdf](https://www.citepa.org/wp-content/uploads/publications/cee-nu/UNECE_France_mars2022.pdf), last access 24 Feb 2023.
- 471 Clarisse, L., Van Damme, M., Hurtmans, D., Franco, B., Clerbaux, C., & Coheur, P.-F.: The diel cycle of  
472 NH<sub>3</sub> observed from the FY-4A Geostationary Interferometric Infrared Sounder (GIIRS). *Geophysical*  
473 *Research Letters*, 48, e2021GL093010, <https://doi.org/10.1029/2021GL093010>, 2021.
- 474 Clarisse, L., Clerbaux, C., Dentener, F., Hurtmans, D., and Coheur, P.-F.: Global ammonia distribution  
475 derived from infrared satellite observations, *Nat. Geosci.*, 2, 479–483,  
476 <https://doi.org/10.1038/ngeo551>, 2009.
- 477 Clerbaux, C., Boynard, A., Clarisse, L., George, M., Hadji-Lazaro, J., Herbin, H., Hurtmans, D., Pommier,  
478 M., Razavi, A., Turquety, S., Wespes, C. and Coheur, P.-F.: Monitoring of atmospheric composition using  
479 the thermal infrared IASI/MetOp sounder, *Atmos. Chem. Phys.*, 9(16), 6041–6054, doi:10.5194/acp-9-  
480 6041-2009, 2009.



- 481 Copernicus Climate Change Service, Climate Data Store, (2023): ERA5 hourly data on single levels from  
482 1940 to present. Copernicus Climate Change Service (C3S) Climate Data Store (CDS), DOI:  
483 10.24381/cds.adbb2d47 (Accessed on 11-May-2023)
- 484 Dammers, E., McLinden, C. A., Griffin, D., Shephard, M. W., Van Der Graaf, S., Lutsch, E., Schaap, M.,  
485 Gainairu-Matz, Y., Fioletov, V., Van Damme, M., Whitburn, S., Clarisse, L., Cady-Pereira, K., Clerbaux,  
486 C., Coheur, P. F., and Erisman, J. W.: NH<sub>3</sub> emissions from large point sources derived from CrIS and IASI  
487 satellite observations, *Atmos. Chem. Phys.*, 19, 12261–12293, [https://doi.org/10.5194/acp-19-12261-](https://doi.org/10.5194/acp-19-12261-2019)  
488 2019, 2019.
- 489 Evangeliou, N., Balkanski, Y., Eckhardt, S., Cozic, A., Van Damme, M., Coheur, P.-F., Clarisse, L.,  
490 Shephard, M. W., Cady-Pereira, K. E. and Hauglustaine, D.: 10-year satellite-constrained fluxes of  
491 ammonia improve performance of chemistry transport models, *Atmos. Chem. Phys.*, 21(6), 4431–  
492 4451, doi:10.5194/acp-21-4431-2021, 2021.
- 493 Farren, N. J., Davison, J., Rose, R. A., Wagner, R. L. and Carslaw, D. C.: Underestimated Ammonia  
494 Emissions from Road Vehicles, *Environ. Sci. Technol.*, 54(24), 15689–15697,  
495 doi:10.1021/acs.est.0c05839, 2020.
- 496 Favez, O., Weber, S., Petit, J.-E., Alleman, L. Y., Albinet, A., Riffault, V., Chazeau, B., Amodeo, T.,  
497 Salameh, D., Zhang, Y., Srivastava, D., Samaké, A., Aujay-Plouzeau, R., Papin, A., Bonnaire, N.,  
498 Boullanger, C., Chatain, M., Chevrier, F., Detournay, A., Leoz-Garziandia, E. (2021). Overview of the  
499 French Operational Network for In Situ Observation of PM Chemical Composition and Sources in Urban  
500 Environments (CARA Program), *Atmosphere*, 12(2), <https://doi.org/10.3390/atmos12020207>, 2021.
- 501 Fortems-Cheiney, A., Dufour, G., Dufossé, K., Couvidat, F., Gilliot, J.-M., Siour, G., Beekmann, M., Foret,  
502 G., Meleux, F., Clarisse, L., Coheur, P.-F., Van Damme, M., Clerbaux, C., and Génarmont, S.: Do  
503 alternative inventories converge on the spatiotemporal representation of spring ammonia emissions  
504 in France?, *Atmos. Chem. Phys.*, 20, 13481–13495, <https://doi.org/10.5194/acp-20-13481-2020>, 2020.
- 505 Fowler, D., et al.: The global nitrogen cycle in the twenty-first century, *Philos. Trans. R. Soc. B*,  
506 368(1621), 1–13, doi:10.1098/rstb.2013.0164, 2013.
- 507 Ge, X., Schaap, M., Kranenburg, R., Segers, A., Reinds, G. J., Kros, H. and de Vries, W.: Modeling  
508 atmospheric ammonia using agricultural emissions with improved spatial variability and temporal  
509 dynamics, *Atmos. Chem. Phys.*, 20(24), 16055–16087, doi:10.5194/acp-20-16055-2020, 2020.
- 510 Guo, X., Wang, R., Pan, D., Zondlo, M. A., Clarisse, L., Van Damme, M., Whitburn, S., Coheur, P.-F.,  
511 Clerbaux, C., Franco, B., Golston, L. M., Wendt, L., Sun, K., Tao, L., Miller, D., Mikoviny, T., Müller, M.,  
512 Wisthaler, A., Tevlin, A. G., Murphy, J. G., Nowak, J. B., Roscioli, J. R., Volkamer, R., Kille, N., Neuman,  
513 J. A., Eilerman, S. J., Crawford, J. H., Yacovitch, T. I., Barrick, J. D. and Scarino, A. J.: Validation of IASI  
514 Satellite Ammonia Observations at the Pixel Scale Using In Situ Vertical Profiles, *J. Geophys. Res.*  
515 *Atmos.*, 126(9), e2020JD033475, doi:<https://doi.org/10.1029/2020JD033475>, 2021.
- 516 Hersbach, H.; Bell, B.; Berrisford, P.; Hirahara, S.; Horányi, A.; Muñoz-Sabater, J.; Nicolas, J.; Peubey,  
517 C.; Radu, R.; Schepers, D.; et al. The ERA5 global reanalysis. *Q. J. R. Meteorol. Soc.* 146, 1999–2049,  
518 doi:10.1002/qj.3803, <https://www.ecmwf.int/en/forecasts/datasets/reanalysis-datasets/era5>, 2020.



- 519 Hu, Q., Zhang, L., Evans, G. J. and Yao, X.: Variability of atmospheric ammonia related to potential  
520 emission sources in downtown Toronto, Canada, *Atmos. Environ.*, 99, 365–373,  
521 doi:<https://doi.org/10.1016/j.atmosenv.2014.10.006>, 2014.
- 522 Ianniello, A., Spataro, F., Esposito, G., Allegrini, I., Rantica, E., Ancora, M. P., Hu, M. and Zhu, T.:  
523 Occurrence of gas phase ammonia in the area of Beijing (China), *Atmos. Chem. Phys.*, 10(19), 9487–  
524 9503, doi:[10.5194/acp-10-9487-2010](https://doi.org/10.5194/acp-10-9487-2010), 2010.
- 525 Jeong, U., Kim, J., Lee, H., Jung, J., Kim, Y. J., Song, C. H. and Koo, J.-H.: Estimation of the contributions  
526 of long range transported aerosol in East Asia to carbonaceous aerosol and PM concentrations in  
527 Seoul, Korea using highly time resolved measurements: a PSCF model approach, *J. Environ. Monit.*,  
528 13(7), 1905–1918, doi:[10.1039/C0EM00659A](https://doi.org/10.1039/C0EM00659A), 2011.
- 529 Kutzner, R. D., Cuesta, J., Chelin, P., Petit, J.-E., Ray, M., Landsheere, X., Tournadre, B., Dupont, J.-C.,  
530 Rosso, A., Hase, F., Orphal, J., and Beekmann, M.: Diurnal evolution of total column and surface  
531 atmospheric ammonia in the megacity of Paris, France, during an intense springtime pollution episode,  
532 *Atmos. Chem. Phys.*, 21, 12091–12111, <https://doi.org/10.5194/acp-21-12091-2021>, 2021.
- 533 Lan, Z., Lin, W., Pu, W. and Ma, Z.: Measurement report: Exploring NH<sub>3</sub> behavior in urban and suburban  
534 Beijing: comparison and implications, *Atmos. Chem. Phys.*, 21(6), 4561–4573, doi:[10.5194/acp-21-4561-2021](https://doi.org/10.5194/acp-21-4561-2021), 2021.
- 536 Li, Y., Thompson, T. M., Van Damme, M., Chen, X., Benedict, K. B., Shao, Y., Day, D., Boris, A., Sullivan,  
537 A. P., Ham, J., Whitburn, S., Clarisse, L., Coheur, P.-F. and Collett Jr., J. L.: Temporal and spatial variability  
538 of ammonia in urban and agricultural regions of northern Colorado, United States, *Atmos. Chem. Phys.*,  
539 17(10), 6197–6213, doi:[10.5194/acp-17-6197-2017](https://doi.org/10.5194/acp-17-6197-2017), 2017.
- 540 Lonati, G. and Cernuschi, S.: Temporal and spatial variability of atmospheric ammonia in the Lombardy  
541 region (Northern Italy), *Atmos. Pollut. Res.*, 11(12), 2154–2163,  
542 doi:<https://doi.org/10.1016/j.apr.2020.06.004>, 2020.
- 543 Lonsdale, C. R., Hegarty, J. D., Cady-Pereira, K. E., Alvarado, M. J., Henze, D. K., Turner, M. D., Capps, S.  
544 L., Nowak, J. B., Neuman, J. A., Middlebrook, A. M., Bahreini, R., Murphy, J. G., Markovic, M. Z.,  
545 VandenBoer, T. C., Russell, L. M., and Scarino, A. J.: Modeling the diurnal variability of agricultural  
546 ammonia in Bakersfield, California, during the CalNex campaign, *Atmos. Chem. Phys.*, 17, 2721–2739,  
547 <https://doi.org/10.5194/acp-17-2721-2017>, 2017.
- 548 Loubet, B., Buysse, P., Gonzaga-Gomez, L., Lafouge, F., Ciuraru, R., Decuq, C., Kammer, J., Bsaibes, S.,  
549 Boissard, C., Durand, B., Gueudet, J.-C., Fanucci, O., Zurfluh, O., Abis, L., Zannoni, N., Truong, F.,  
550 Baisnée, D., Sarda-Estève, R., Staudt, M. and Gros, V.: Volatile organic compound fluxes over a winter  
551 wheat field by PTR-Qi-TOF-MS and eddy covariance, *Atmos. Chem. Phys.*, 22(4), 2817–2842,  
552 doi:[10.5194/acp-22-2817-2022](https://doi.org/10.5194/acp-22-2817-2022), 2022.
- 553 Ludemann, C. I., Gruere, A., Heffer, P. and Dobermann, A.: Global data on fertilizer use by crop and  
554 by country, *Sci. Data*, 9(1), 501, doi:[10.1038/s41597-022-01592-z](https://doi.org/10.1038/s41597-022-01592-z), 2022.
- 555 Malm, W. C., Johnson, C. E., and Bresch, J. F.: Application of principal component analysis for purpose  
556 of identifying source receptor relationships, in *Receptor Methods for Source Apportionment*, Pace,  
557 T.G., Ed.; Publication TR-5, Air Pollution Control Association, Pittsburgh, PA, pp. 127–148, 1986.
- 558 Marais, E. A., Pandey, A. K., Van Damme, M., Clarisse, L., Coheur, P.-F., Shephard, M. W., Cady-Pereira,  
559 K. E., Misselbrook, T., Zhu, L., Luo, G. and Yu, F.: UK Ammonia Emissions Estimated With Satellite



- 560 Observations and GEOS-Chem, *J. Geophys. Res. Atmos.*, 126(18), e2021JD035237,  
561 doi:<https://doi.org/10.1029/2021JD035237>, 2021.
- 562 Martino, M., Tassone, A., Angiuli, L., Naccarato, A., Dambruoso, P. R., Mazzone, F., Trizio, L., Leonardi,  
563 C., Petracchini, F., Sprovieri, F., Pirrone, N., D'Amore, F. and Bencardino, M.: First atmospheric mercury  
564 measurements at a coastal site in the Apulia region: seasonal variability and source analysis, *Environ.*  
565 *Sci. Pollut. Res.*, 29(45), 68460–68475, doi:10.1007/s11356-022-20505-6, 2022.
- 566 McDuffie, E. E., Smith, S. J., O'Rourke, P., Tibrewal, K., Venkataraman, C., Marais, E. A., Zheng, B.,  
567 Crippa, M., Brauer, M., and Martin, R. V.: A global anthropogenic emission inventory of atmospheric  
568 pollutants from sector- and fuel-specific sources (1970–2017): an application of the Community  
569 Emissions Data System (CEDS), *Earth Syst. Sci. Data*, 12, 3413–3442, <https://doi.org/10.5194/essd-12-3413-2020>, 2020.
- 571 Nair, A. A. and Yu, F.: Quantification of Atmospheric Ammonia Concentrations: A Review of Its  
572 Measurement and Modeling, *Atmosphere (Basel)*, 11(10), doi:10.3390/atmos11101092, 2020.
- 573 Osada, K.: Measurement report: Short-term variation in ammonia concentrations in an urban area  
574 increased by mist evaporation and emissions from a forest canopy with bird droppings, *Atmos. Chem.*  
575 *Phys.*, 20, 11941–11954, <https://doi.org/10.5194/acp-20-11941-2020>, 2020.
- 576 Pazmiño, A., Beekmann, M., Goutail, F., Ionov, D., Bazureau, A., Nunes-Pinharanda, M., Hauchecorne,  
577 A., and Godin-Beekmann, S.: Impact of the COVID-19 pandemic related to lockdown measures on  
578 tropospheric NO<sub>2</sub> columns over Île-de-France, *Atmos. Chem. Phys.*, 21, 18303–18317,  
579 <https://doi.org/10.5194/acp-21-18303-2021>, 2021.
- 580 Perrino, C., Catrambone, M., Di Menno Di Bucchianico, A. and Allegrini, I.: Gaseous ammonia in the  
581 urban area of Rome, Italy and its relationship with traffic emissions, *Atmos. Environ.*, 36(34), 5385–  
582 5394, doi:[https://doi.org/10.1016/S1352-2310\(02\)00469-7](https://doi.org/10.1016/S1352-2310(02)00469-7), 2002.
- 583 Petetin, H., et al.: Assessing the ammonium nitrate formation regime in the Paris megacity and its  
584 representation in the CHIMERE model, *Atmos. Chem. Phys.*, 16, 10419–10440, doi:10.5194/acp-16-  
585 10419-2016, 2016.
- 586 Pu, W., Sheng, J., Tian, P., Huang, M., Liu, X., Collett, J. L., Li, Z., Zhao, X., He, D., Dong, F., Zhang, N.,  
587 Quan, W., Qiu, Y., Song, Y., Lin, W., Pan, Y. and Ma, Z.: On-road mobile mapping of spatial variations  
588 and source contributions of ammonia in Beijing, China, *Sci. Total Environ.*, 864, 160869,  
589 doi:<https://doi.org/10.1016/j.scitotenv.2022.160869>, 2023.
- 590 Pope III, C. A., et al.: Fine-particulate air pollution and life expectancy in the United States, *N. Engl. J.*  
591 *Med.*, 360(4), 376–386, doi:10.1056/NEJMsa0805646, 2009.
- 592 Qadri, A. M., Singh, G. K., Paul, D., Gupta, T., Rabha, S., Islam, N. and Saikia, B. K.: Variabilities of  $\delta^{13}C$   
593 and carbonaceous components in ambient PM<sub>2.5</sub> in Northeast India: Insights into sources and  
594 atmospheric processes, *Environ. Res.*, 214, 113801,  
595 doi:<https://doi.org/10.1016/j.envres.2022.113801>, 2022.
- 596 Ren, B., Xie, P., Xu, J., Li, A., Tian, X., Hu, Z., Huang, Y., Li, X., Zhang, Q., Ren, H. and Ji, H.: Use of the  
597 PSCF method to analyze the variations of potential sources and transports of NO<sub>2</sub>, SO<sub>2</sub>, and HCHO  
598 observed by MAX-DOAS in Nanjing, China during 2019, *Sci. Total Environ.*, 782, 146865,  
599 doi:<https://doi.org/10.1016/j.scitotenv.2021.146865>, 2021.



- 600 Rockström, J., Steffen, W., Noone, K., Persson, Å., Chapin, F. S., Lambin, E. F., Lenton, T. M., Scheffer,  
601 M., Folke, C., Schellnhuber, H. J., Nykvist, B., de Wit, C. A., Hughes, T., van der Leeuw, S., Rodhe, H.,  
602 Sörlin, S., Snyder, P. K., Costanza, R., Svedin, U., Falkenmark, M., Karlberg, L., Corell, R. W., Fabry, V. J.,  
603 Hansen, J., Walker, B., Liverman, D., Richardson, K., Crutzen, P. and Foley, J. A.: A safe operating space  
604 for humanity, *Nature*, 461(7263), 472–475, doi:10.1038/461472a, 2009.
- 605 Roe, S.; Spivey, M.; Lindquist, H.; Thesing, K.; Strait, R.; Pechan, E.; Associates, I. Estimating Ammonia  
606 Emissions from Anthropogenic Nonagricultural Sources. EPA Emission Inventory Improvement  
607 Program. Technical Report; Emission Inventory Improvement Program, 2004.
- 608 Shephard, M.W., and Cady-Pereira, K.E.: Cross-track Infrared Sounder (CrIS) satellite observations of  
609 tropospheric ammonia, *Atmos. Meas. Tech.*, 8, 1323-1336, 2015.
- 610 Stein, A. F., Draxler, R. R., Rolph, G. D., Stunder, B. J. B., Cohen, M. D. and Ngan, F.: NOAA's HYSPLIT  
611 Atmospheric Transport and Dispersion Modeling System, *Bull. Am. Meteorol. Soc.*, 96(12), 2059–2077,  
612 doi:10.1175/BAMS-D-14-00110.1, 2015.
- 613 Sudesh, S, and Kulshrestha, U. C. Diurnal Variation of Ambient NH<sub>3</sub> in Relation with Agricultural  
614 Activities and Meteorological Factors at a Rural Site in North India. *Curr World Environ*, SI1.  
615 DOI:<http://dx.doi.org/10.12944/CWE.16.Special-Issue1.02>, 2021.
- 616 Sun, K., Tao, L., Miller, D. J., Pan, D., Golston, L. M., Zondlo, M. A., Griffin, R. J., Wallace, H. W., Leong,  
617 Y. J., Yang, M. M., Zhang, Y., Mauzerall, D. L. and Zhu, T.: Vehicle Emissions as an Important Urban  
618 Ammonia Source in the United States and China, *Environ. Sci. Technol.*, 51(4), 2472–2481,  
619 doi:10.1021/acs.est.6b02805, 2017.
- 620 Sutton, M. A., Reis, S., Riddick, S. N., Dragosits, U., Nemitz, E., Theobald, M. R., Tang, Y. S., Braban, C.  
621 F., Vieno, M., Dore, A. J., Mitchell, R. F., Wanless, S., Daunt, F., Fowler, D., Blackall, T. D., Milford, C.,  
622 Flechard, C. R., Loubet, B., Massad, R., Cellier, P., Personne, E., Coheur, P. F., Clarisse, L., Van Damme,  
623 M., Ngadi, Y., Clerbaux, C., Skjøth, C. A., Geels, C., Hertel, O., Wichink Kruit, R. J., Pinder, R. W., Bash, J.  
624 O., Walker, J. T., Simpson, D., Horváth, L., Misselbrook, T. H., Bleeker, A., Dentener, F. and de Vries, W.:  
625 Towards a climate-dependent paradigm of ammonia emission and deposition, *Philos. Trans. R. Soc.*  
626 *Lond. B. Biol. Sci.*, 368(1621), 20130166, doi:10.1098/rstb.2013.0166, 2013.
- 627 Sutton, M.; Dragosits, U.; Tang, Y.; Fowler, D.: Ammonia emissions from nonagricultural sources in the  
628 UK. *Atmos. Environ.* 34, 855– 869, DOI: 10.1016/S1352-2310(99)00362-3, 2000.
- 629 Twigg, M. M., Berkhout, A. J. C., Cowan, N., Crunaire, S., Dammers, E., Ebert, V., Gaudion, V., Haaima,  
630 M., Häni, C., John, L., Jones, M. R., Kamps, B., Kentisbeer, J., Kupper, T., Leeson, S. R., Leuenberger, D.,  
631 Lüttschwager, N. O. B., Makkonen, U., Martin, N. A., Missler, D., Mounsor, D., Neftel, A., Nelson, C.,  
632 Nemitz, E., Oudwater, R., Pascale, C., Petit, J.-E., Pogany, A., Redon, N., Sintermann, J., Stephens, A.,  
633 Sutton, M. A., Tang, Y. S., Zijlmans, R., Braban, C. F., and Niederhauser, B.: Intercomparison of in situ  
634 measurements of ambient NH<sub>3</sub>: instrument performance and application under field conditions,  
635 *Atmos. Meas. Tech.*, 15, 6755–6787, <https://doi.org/10.5194/amt-15-6755-2022>, 2022.
- 636 Van Damme, M., Clarisse, L., Stavrou, T., Wichink Kruit, R., Sellekaerts, L., Viatte, C., Clerbaux, C. and  
637 Coheur, P.-F.: On the weekly cycle of atmospheric ammonia over European agricultural hotspots, *Sci.*  
638 *Rep.*, 12(1), 12327, doi:10.1038/s41598-022-15836-w, 2022.



- 639 Van Damme, M., Clarisse, L., Franco, B., Sutton, M. A., Erisman, J. W., Wichink Kruit, R., van Zanten,  
640 M., Whitburn, S., Hadji-Lazaro, J., Hurtmans, D., Clerbaux, C., & Coheur, P.-F.: Global, regional and  
641 national trends of atmospheric ammonia derived from a decadal (2008–2018) satellite record.  
642 *Environmental Research Letters*, 16(5), 55017. <https://doi.org/10.1088/1748-9326/abd5e0>, 2021.
- 643 Van Damme, M., Clarisse, L., Whitburn, S., Hadji-Lazaro, J., Hurtmans, D., Clerbaux, C. and Coheur, P.-  
644 F.: Industrial and agricultural ammonia point sources exposed, *Nature*, 564(7734), 99–103,  
645 doi:10.1038/s41586-018-0747-1, 2018.
- 646 Van Damme, M., Clarisse, L., Dammers, E., Liu, X., Nowak, J. B., Clerbaux, C., Flechard, C. R., Galy-  
647 Lacaux, C., Xu, W., Neuman, J. A., Tang, Y. S., Sutton, M. A., Erisman, J. W. and Coheur, P. F.: Towards  
648 validation of ammonia (NH<sub>3</sub>) measurements from the IASI satellite, *Atmos. Meas. Tech.*, 8(3), 1575–  
649 1591, doi:10.5194/amt-8-1575-2015, 2015.
- 650 Viatte, C. (2023). NH<sub>3</sub> from Mini Doas [Data set]. LATMOS.
- 651 Viatte, C., Abeer, R., Yamanouchi, S., Porter, W. C., Safieddine, S., Van Damme, M., Clarisse, L., Herrera,  
652 B., Grutter, M., Coheur, P.-F., Strong, K. and Clerbaux, C.: NH<sub>3</sub> spatiotemporal variability over Paris,  
653 Mexico City, and Toronto, and its link to PM<sub>2.5</sub> during pollution events, *Atmos. Chem. Phys.*, 22(19),  
654 12907–12922, doi:10.5194/acp-22-12907-2022, 2022.
- 655 Viatte, C., Petit, J.-E., Yamanouchi, S., Van Damme, M., Doucerain, C., Germain-Piaulenne, E., Gros, V.,  
656 Favez, O., Clarisse, L., Coheur, P.-F., Strong, K. and Clerbaux, C.: Ammonia and PM<sub>2.5</sub> air pollution in  
657 paris during the 2020 covid lockdown, *Atmosphere*, 12(2), doi:10.3390/atmos12020160, 2021.
- 658 Viatte, C., Wang, T., Van Damme, M., Dammers, E., Meleux, F., Clarisse, L., Shephard, M. W., Whitburn,  
659 S., François Coheur, P., Cady-Pereira, K. E. and Clerbaux, C.: Atmospheric ammonia variability and link  
660 with particulate matter formation: A case study over the Paris area, *Atmos. Chem. Phys.*, 20(1),  
661 doi:10.5194/acp-20-577-2020, 2020.
- 662 Volten, H., Bergwerff, J. B., Haaima, M., Lolkema, D. E., Berkhout, A. J. C., van der Hoff, G. R., Potma,  
663 C. J. M., Wichink Kruit, R. J., van Pul, W. A. J. and Swart, D. P. J.: Two instruments based on differential  
664 optical absorption spectroscopy (DOAS) to measure accurate ammonia concentrations in the  
665 atmosphere, *Atmos. Meas. Tech.*, 5(2), 413–427, doi:10.5194/amt-5-413-2012, 2012.
- 666 von Bobruzki, K., Braban, C. F., Famulari, D., Jones, S. K., Blackall, T., Smith, T. E. L., Blom, M., Coe, H.,  
667 Gallagher, M., Ghalaieny, M., McGillen, M. R., Percival, C. J., Whitehead, J. D., Ellis, R., Murphy, J.,  
668 Mohacsi, A., Pogany, A., Junninen, H., Rantanen, S., Sutton, M. A. and Nemitz, E.: Field inter-  
669 comparison of eleven atmospheric ammonia measurement techniques, *Atmos. Meas. Tech.*, 3(1), 91–  
670 112, doi:10.5194/amt-3-91-2010, 2010.
- 671 Wang, B., Liu, Z., Li, Z., Sun, Y., Wang, C., Zhu, C., Sun, L., Yang, N., Bai, G., Fan, G., Sun, X., Xia, Z., Pan,  
672 G., Xu, C. and Yan, G.: Characteristics, chemical transformation and source apportionment of volatile  
673 organic compounds (VOCs) during wintertime at a suburban site in a provincial capital city, east China,  
674 *Atmos. Environ.*, 298, 119621, doi:<https://doi.org/10.1016/j.atmosenv.2023.119621>, 2023.





- 675 Wang, S., Nan, J., Shi, C., Fu, Q., Gao, S., Wang, D., Cui, H., Saiz-Lopez, A. and Zhou, B.: Atmospheric  
676 ammonia and its impacts on regional air quality over the megacity of Shanghai, China, *Sci. Rep.*, 5(1),  
677 15842, doi:10.1038/srep15842, 2015.
- 678 Wang, Y.Q., Zhang, X.Y. and Draxler, R.:TrajStat: GIS-based software that uses various trajectory  
679 statistical analysis methods to identify potential sources from long-term air pollution measurement  
680 data. *Environmental Modelling & Software*, 24: 938-939, 2009.
- 681 Warner, J. X., Wei, Z., Strow, L. L., Dickerson, R. R., and Nowak, J. B.: The global tropospheric ammonia  
682 distribution as seen in the 13-year AIRS measurement record, *Atmos. Chem. Phys.*, 16, 5467-5479,  
683 <https://doi.org/10.5194/acp-16-5467-2016>, 2016.
- 684 Wen, Y., Zhang, S., Wu, Y. and Hao, J.: Vehicular ammonia emissions: An underappreciated emission  
685 source in densely-populated areas, *Atmos. Chem. Phys. Discuss.*, 2022, 1–14, doi:10.5194/acp-2022-  
686 828, 2022.
- 687 Whitehead, J., Longley, D., Coe, H. and Gallagher, M.: Hourly concentrations of ammonia during the  
688 winter in Manchester, UK, related to traffic and background sources, Fifth Conference on Urban  
689 Environment, Session 14 urban air quality (including urban airshed modeling and urban air chemistry  
690 experiments), Vancouver BC, Canada, 23-26 August 2004.
- 691 Zachary, M., Yin, L. and Zacharia, M.: Application of PSCF and CWT to Identify Potential Sources of  
692 Aerosol Optical Depth in ICIPE Mbita. *Open Access Library Journal*, 5, 1-12. doi: 10.4236/oalib.1104487,  
693 2018.
- 694 Zhang, Q., Wei, N., Zou, C. and Mao, H.: Evaluating the ammonia emission from in-use vehicles using  
695 on-road remote sensing test, *Environ. Pollut.*, 271, 116384,  
696 doi:<https://doi.org/10.1016/j.envpol.2020.116384>, 2021.